Modeling of pseudotwinning in Fe_3Ga

2014 Modelling Simul. Mater. Sci. Eng. 22 055008

(http://iopscience.iop.org/0965-0393/22/5/055008)

IOP Publishing Modelling and Simulation in Materials Science and Engineering

Modelling Simul. Mater. Sci. Eng. **22** (2014) 055008 (18pp) doi:10.1088/0965-0393/22/5/055008

Modeling of pseudotwinning in Fe_3Ga

J Wang and H Sehitoglu[1]

Department of Mechanical Science and Engineering, University of Illinois at Urbana-Champaign, 1206 West Green Street, Urbana, IL 61801, USA

E-mail: huseyin@illinois.edu

Received 16 November 2013, revised 22 March 2014
Accepted for publication 11 April 2014
Published 15 May 2014

Abstract

Pseudotwinning is an important deformation mechanism that can produce reversible deformations similar to the shape memory phenomenon. Pseudotwinning merits further consideration from a modeling viewpoint as it could open new frontiers for discovery of alloys with recoverability of deformation. In this study, we focus on the Fe_3Ga ($D0_3$ and $L1_2$ lattices) with atomistic simulations. We present a pseudotwin nucleation model based on the generalized planar fault energy from first-principles calculations. The minimization of the total energy at the mesoscale associated with pseudotwin nucleation leads to determination of the twinning stress. The low energy barriers and twinning stress demonstrate that pseudotwinning in $D0_3$ Fe_3Ga is a possible deformation mode, but pseudotwinning is unlikely to occur in $L1_2$ Fe_3Ga due to the significantly high energy barrier and twinning stress. The predicted twinning stress is compared with experimental measurements, and the results show very good agreement. Hence, we suggest that the results provide a quantitative methodology to understanding and determining pseudotwinning in ordered alloys.

Keywords: pseudotwinning, critical stress, twinning, density functional theory, reversible deformation

(Some figures may appear in colour only in the online journal)

1. Introduction

1.1. Fundamentals of pseudotwinning

Twinning is an important plastic deformation mode in metals and alloys. It can have two forms: 'true' and 'pseudo' twins [1, 2]. For a true twin, the lattice sites in twin positions

[1] Author to whom any correspondence should be addressed.

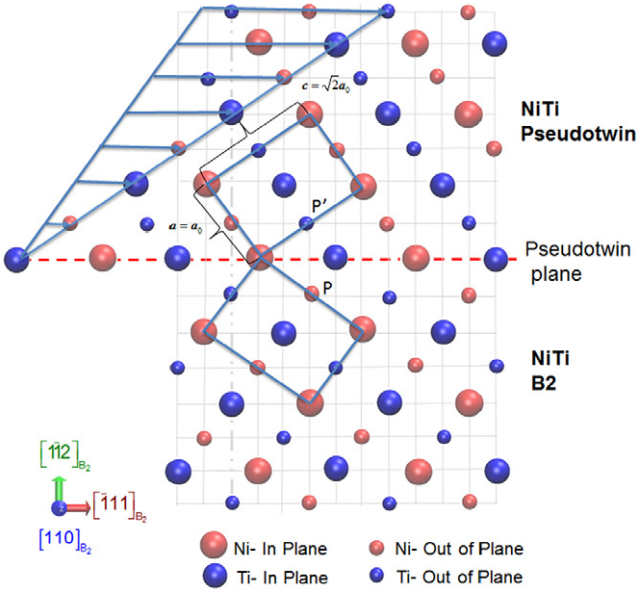

Figure 1. Simple demonstration of pseudotwinning in B2 alloys (the NiTi example). Successive shear on seven layers is shown. Illustration of shearing in B2 structure resulting in a transition from cubic to orthorhombic phase. The twin that results is not reflective (P and P′ are unlike atoms) and is termed a 'pseudotwin'. The resulting orthorhombic structure has lattice parameters $a = a_0$ and $c = \sqrt{2}a_0$, where a_0 is the lattice parameter of the B2 structure. The red and blue atoms represent Ni and Ti, respectively. The different size of atoms indicates atoms are in plane and out of plane.

are occupied by the same species of atoms, which maintain the same atomic arrangements in the matrix and twin. In contrast, the lattice sites in twin positions of a pseudotwin are occupied by different species of atoms, which results in incorrect atomic arrangements—atoms of the matrix and pseudotwin are not a mirror reflection. The formation of pseudotwins and the return to the original structure upon unloading can have very important consequences in plasticity of metals. Despite its importance, it has received little attention and this study is focused on identifying the key parameters that govern pseudotwinning via modeling efforts.

Pseudotwinning [3–7], originally proposed by Laves [8] and developed by Cahn [9], results in an orthorhombic structure (O-phase) in the case of B2 alloys, hence the term 'pseudo-' was coined [10]. To be completely accurate in definitions, the pseudotwin formation is not a twin since a 'new' phase is formed during the twinning shear. For ordered B2 alloys, the pseudotwin operation can be viewed as a stress-induced martensitic transformation, where, upon shearing, a new O-phase is obtained [11–13]. An illustration of pseudotwinning for cubic NiTi (B2) after shearing of seven $(1\,\bar{1}\,2)$ layers along $[\bar{1}\,1\,1]$ direction is shown in figure 1. The NiTi pseudotwin structure has the lattice parameters $a = a_0$ and $c = \sqrt{2}a_0$, where a_0 is the lattice parameter of the B2 structure. We note the presence of unlike atoms P and P′ across the interface. This is called a 'pseudotwin' as opposed to a 'reflective' twin. For an ordered alloy such as NiTi, the twinning operation can be viewed as a martensitic transformation [11]. It has also been referred to as some form of disordering, because after shearing, 50% of the nearest neighbors become unlike pairs. To revert to the original structure with a perfect reflection, twin

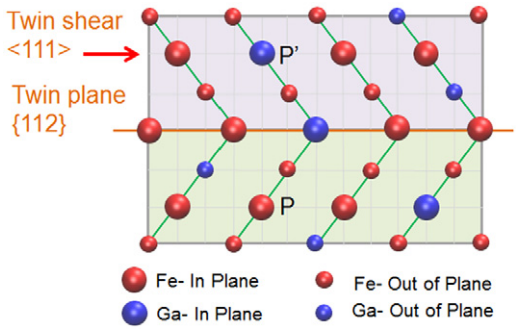

Figure 2. Schematic of pseudotwinning in $D0_3$ Fe_3Ga with the twin plane $\{1\,1\,2\}$ (brown line) and twin direction $\langle 1\,1\,1\rangle$ (red arrow). The unlike atoms P (Fe) and P′ (Ga) across the twin plane form the pseudotwinning. The red and blue atoms represent Fe and Ga, respectively. Different sizes of atoms represent in plane and out of plane from the top view.

atoms need to exchange places (along $[\bar{1}\,1\,1]$), a process referred to as a 'shuffle'. In the absence of this shuffle, this crystal structure has different lattice parameters as shown in figure 1.

The observation of $\{1\,1\,2\}\langle 1\,1\,\bar{1}\rangle$ pseudotwin in the mechanically deformed B2 NiTi has been reported in B2 NiTi alloys [1, 4]. However, through atomistic simulations, the energy barrier associated with the $(\bar{2}\,1\,1)[\bar{1}\,\bar{1}\,\bar{1}]$ pseudotwin in NiTi is calculated to be rather high ($500\,\mathrm{mJ\,m^{-2}}$), and continues to increase during the process of twin growth [14]. Pseudotwinning in the form of O-phase is either mechanically unstable (there is a very large total energy difference between B2 and O-phase, ΔE) or metastable but with a large ΔE requiring a large stress to propagate the pseudotwin [15]. It is clear from the above considerations that pseudotwinning could be a possible mechanism in alloys where the energy magnitudes do not build up layer after layer during growth of the pseudotwin. Therefore, in the case of the Fe_3Ga alloys, our purpose is to study the development of the twin layers and the accompanying energy barriers.

1.2. Pseudotwinning in Fe_3Ga

Recently, pseudotwinning was experimentally reported in single crystals of $D0_3Fe_3Ga$ and shown to become more significant as the deformation temperature was decreased [16, 17]. The pseudotwin can generate a larger recoverable strain upon unloading, so it is a possible venue to increase the ductility of Fe_3Ga [18]. Figure 2 shows the pseudotwin in $D0_3Fe_3Ga$ with the twin plane as $\{1\,1\,2\}$ and the twin direction as $\langle 1\,1\,1\rangle$. We note the presence of unlike atoms P (Fe) and P′ (Ga) across the interface. This is identified as a 'pseudotwin' as opposed to a 'reflective' twin.

There is a lack of theoretical work to understand pseudotwin formation in $D0_3Fe_3Ga$ and to calculate the associated energy barrier. The generalized planar fault energy (GPFE) provides a comprehensive description of twins, which is the energy per unit area required to form n-layer twins by shearing n consecutive layers along twinning direction [19–22]. Upon establishing the GPFE curve in $D0_3$ Fe_3Ga, we calculate the critical shear stress for twin nucleation through the model based on Peierls–Nabarro (P–N) concepts [23–26] and compare with available experimental values. From the Fe–Ga phase equilibrium diagram we note that the $D0_3$ single-phase region forms around 600 °C while $L1_2$ can develop below 600 °C [27]. The possible occurrence of $L1_2$ structure may affect the deformation behavior of Fe_3Ga since it

presents a different magnitude level of twinning stress compared to $D0_3$. Thus, it is important to theoretically study the deformation behavior of $L1_2$ Fe_3Ga, and to determine its GPFE and compare with $D0_3$ structure.

The pseudotwin is a possible deformation mode in an ordered lattice, and this is an important topic since pseudotwinning is a possible means of increasing the ductility of ordered lattices [28]. The purpose of this paper is to establish a pseudotwin nucleation model incorporating atomistic simulations to develop a general methodology for understanding pseudotwinning in Fe_3Ga, and compare the results with experiments.

2. Simulations

The first-principles density functional theory (DFT) calculations were carried out to calculate the system's total energy [29, 30]. We utilized the Vienna Ab-initio Simulations Package (VASP) with the projector augmented wave (PAW) method and the generalized gradient approximation (GGA) as implementations of DFT [31, 32]. In our calculations, we used $9 \times 9 \times 9$ Monkhorst–Pack k-point meshes for the Brillouin-zone integration to ensure the convergence of results. Ionic relaxation was performed by a conjugate gradient algorithm and stopped when absolute values of internal forces were smaller than 5×10^{-3} eV Å^{-1}. The energy cut-off of 500 eV was used for the plane-wave basis set. The total energy was converged to less than 10^{-5} eV per atom. For GPFE calculations a full internal atom relaxation, including perpendicular and parallel directions to the fault plane, was allowed for, minimizing the short-range interaction between misfitted layers near to the fault plane. This relaxation process caused a small additional atomic displacement $r(|r| = \sqrt{r_x^2 + r_y^2 + r_z^2})$, and thus the total fault displacement is not exactly equal to the shear displacement, u, but involves additional r [22]. During the relaxation process atoms avoided coming too close to each other [33–35], and the total energy of the deformed (faulted) crystal was minimized.

2.1. Pseudotwin of $D0_3$ Fe_3Ga

The pseudotwinning system $\{1\,1\,2\}\langle 1\,1\,1\rangle$ has been observed experimentally for $D0_3$ structures of Fe_3Ga and Fe_3Al [16, 17]. Figure 3 shows the $\{1\,1\,2\}$ twin plane (shaded violet) and the $\langle 1\,1\,1\rangle$ twin direction (green arrow) in the unit cell of cubic austenite $D0_3$ Fe_3Ga. We note that the lattice parameter a_0 represents repeating atom positions in the $\langle 1\,0\,0\rangle$ directions, and the $D0_3$ unit cell contains eight B2 type subcells. In each subcell the Fe atoms occupy corners and since there are eight subcells, the corner atoms provide eight Fe atoms in the $D0_3$ unit cell. Additionally, four Fe atoms occupy the centers of four subcells, and four Ga atoms occupy the centers of the other four subcells. Thus, the total number of atoms in one $D0_3$ unit cell is sixteen and the atom ratio of Fe to Ga is three.

We conducted simulations to determine the GPFE of $D0_3$ Fe_3Ga by successive shear of every $(1\,\bar{1}\,2)$ plane over $\frac{1}{12}[\bar{1}\,1\,1]$ partial dislocation. The twinning Burgers vector is $b = \frac{\sqrt{3}}{12}a_0$, where $a_0 = 5.83$ Å is the lattice parameter of $D0_3$ Fe_3Ga in good agreement with experiments (table 1). The atomic arrangement of the pseudotwin formation in $D0_3$ Fe_3Ga viewed from the $[1\,1\,0]$ direction is illustrated in figure 4. Figure 4(a) shows the perfect $D0_3$ lattice, while figure 4(b) is the lattice with a seven-layer pseudotwin after shearing seven Burgers vector ($7b$, shown with a green arrow) in successive $(1\,\bar{1}\,2)$ planes (shown in a brown dashed line). The different size of atoms represents two layers of atoms stacking (atoms in plane and out of plane). We note the presence of unlike atoms P (Fe) and P′ (Ga) crossing the interface forms the pseudotwin. Similar to body-centered cubic (bcc) metals, the atomic stacking sequence of

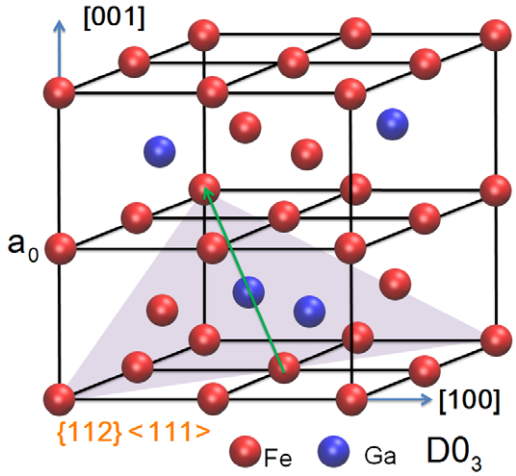

Figure 3. Schematic of the $\{1\,1\,2\}$ twin plane (shaded violet) and the $\langle 1\,1\,1\rangle$ twin direction (green arrow) in the austenite $D0_3Fe_3Ga$ unit cell. The $D0_3$ unit cell contains eight B2 type subcells, and the atom ratio of Fe to Ga is three.

Table 1. The calculated lattice parameter of $D0_3$ and $L1_2$ is compared to experiments. The lattice type of subcell and structural energy are also given.

		Lattice parameter (Å)		Structural energy
Structure of Fe_3Ga	Lattice type	This study	Experiments	(eV/atom)
$D0_3$	bcc	5.83	5.84 [37, 38]	−7.086
$L1_2$	fcc	3.66	3.67 [39]	−7.131

$\{1\,1\,2\}$ plane is ... ABCDEFABC ... [36]. We note that the twinning mechanism is different between bcc metals and $D0_3$ structure. It is well known that after the seven-layer twin is formed, the atomic stacking sequence of ... ABCDEFABC ... in a perfect bcc metal becomes the sequence of ... ABAFEDCBA .... The first letter 'B' in the sequence is assumed as the twin plane, and the $(1\,\bar{1}\,2)$ planes above it are displaced by shearing with $\frac{1}{12}[\bar{1}\,1\,1]$. However, in a perfect $D0_3$ structure the $(1\,\bar{1}\,2)$ planes above the twin plane have the transition C → A′, D → F′, E → E′, A → C′ and B → B′. Here the letters with prime represent the planes with the same lattice sites as planes without prime, but the lattice sites have different species of atoms. Thus, the stacking sequence of ... ABCDEFABC ... in a perfect $D0_3$ structure becomes the sequence of ... ABA′F′E′DC′B′A′ ... in a pseudotwin structure.

Figure 5 shows a unit cell of the pseudotwin structure upon pseudotwinning of $D0_3$ Fe_3Ga. The pseudotwin structure is different to the $D0_3$ parent phase and is orthorhombic with lattice parameters $a = \frac{1}{2}a_0$, $b = \frac{\sqrt{2}}{2}a_0$, $c = \sqrt{2}a_0$. This is similar to pseudotwinning in B2 alloys, where pseudotwinning produces a different phase to B2 structure [12, 15].

We obtained the GPFE curve for $D0_3$ pseudotwinning by shear of consecutive $(1\,\bar{1}\,2)$ layers with displacement, u, which is normalized by the twinning Burgers vector b along $[\bar{1}\,1\,1]$ direction. The calculated energy landscape for a six-layer twin formation in $D0_3$ Fe_3Ga is shown in figure 6. We note that similar to bcc crystals Fe and V [40], $u/b = 1$ is not a metastable position; instead, it possesses the unstable stacking-fault energy (maximum

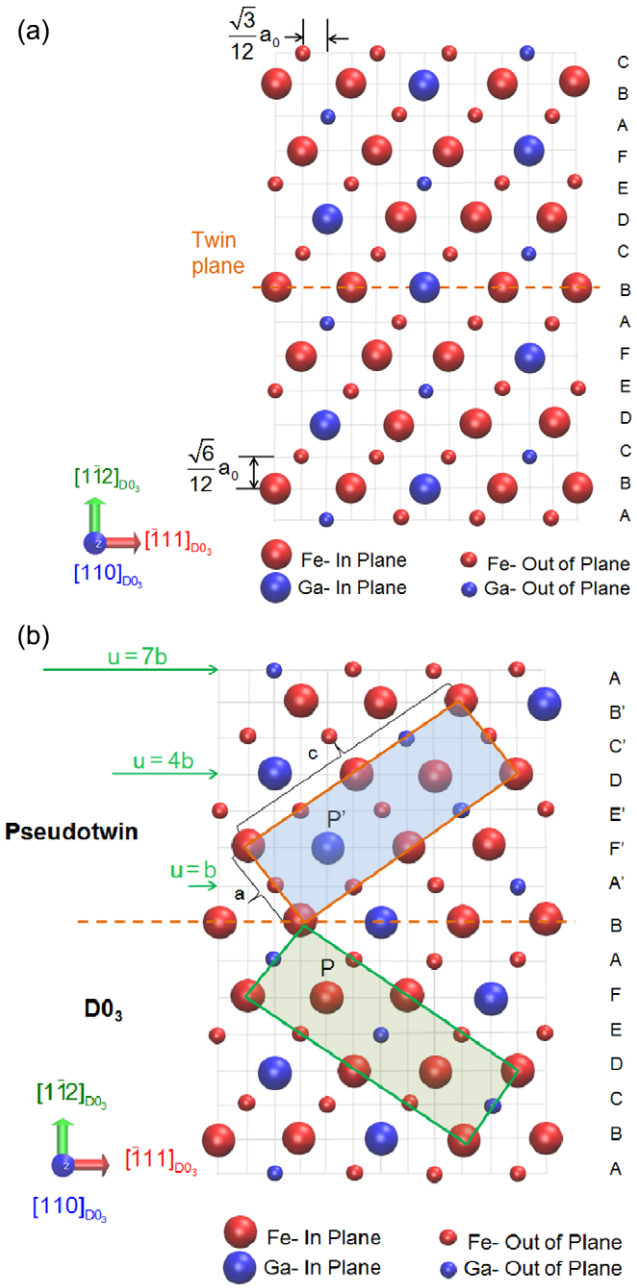

Figure 4. Pseudotwinning in $(1\,\bar{1}\,2)$ plane with $\frac{1}{12}[\bar{1}\,1\,1]$ partial dislocation (twinning Burgers vector $b = 0.84$ Å) of $D0_3$ Fe_3Ga. (*a*) The perfect $D0_3$ lattice viewed from the $[1\,1\,0]$ direction. Twining plane $(1\,\bar{1}\,2)$ is marked with a brown dashed line. The different size of atoms represents two layers of atom stacking (atoms in plane and out of plane). (*b*) The lattice with a seven layer twin after shearing along $\frac{1}{12}[\bar{1}\,1\,1]$ dislocation, u, shown by a green arrow. The pseudotwin structure is different to the $D0_3$ parent phase and is orthorhombic with lattice parameters $a = \frac{1}{2}a_0$, $b = \frac{\sqrt{2}}{2}a_0$, $c = \sqrt{2}a_0$.

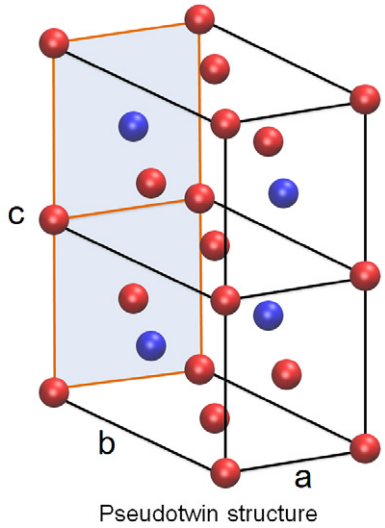

Figure 5. The unit cell of pseudotwin structure of $D0_3$. Upon pseudotwinning, the cubic $D0_3$ changes to the orthorhombic structure with lattice parameters $a = \frac{1}{2}a_0$, $b = \frac{\sqrt{2}}{2}a_0$, and $c = \sqrt{2}a_0$, where a_0 is the lattice parameter of $D0_3$. The light-blue plane corresponds to the plane of pseudotwin structure in figure 4(*b*).

energy barrier of 170 mJ m^{-2}) for emitting the first $\frac{1}{12}[\bar{1}\,1\,1]$ twinning partial from the initial perfect crystal. The metastable and unstable positions are observed at $u/b = \frac{3}{2}, \frac{5}{2}, \frac{7}{2}\ldots$ and $u/b = 2, 3, 4\ldots$, respectively. The shape of the GPFE curve for the emission of subsequent $\frac{1}{12}[\bar{1}\,1\,1]$ partials is not a periodic wave and has different peaks and valleys. However, we note that the difference between a peak and a valley of the curve is almost constant and we define it as a twin migration energy, $\gamma_{\mathrm{TM}} = 50$ mJ m^{-2}. This is the energy barrier for emitting subsequent $\frac{1}{12}[\bar{1}\,1\,1]$ twinning partials on consecutive $(1\,\bar{1}\,2)$ planes in the presence of a pre-existing stacking-fault energy [40, 41].

It is calculated that the energy barriers to form a pseudotwin and to migrate twin boundaries in B2 NiTi is rather high (500 mJ m^{-2} and 300 mJ m^{-2}, respectively [14]), so pseudotwinning is an unlikely deformation mechanism [15]. However, in the case of $D0_3$ Fe_3Ga, the energy barriers of the formation and growth of twinning are 170 mJ m^{-2} and 50 mJ m^{-2}, respectively. These energies are much lower than the case in B2 NiTi, which allows the formation of a pseudotwin in $D0_3$ Fe_3Ga [16].

2.2. Pseudotwin of $L1_2$ Fe_3Ga

The Pseudotwinning system $(1\,1\,1)[\bar{1}\,\bar{1}\,2]$ has been experimentally observed in $L1_2$ structures [42–45]. Figure 7 shows the configuration of pseudotwinning in the plane $(1\,1\,1)$ (shaded violet) with twinning dislocation $\frac{1}{6}[\bar{1}\,\bar{1}\,2]$ (red arrow). We note that in the $L1_2$ unit cell, Ga atoms occupy corner positions and Fe atoms remain at the face center.

We conducted simulations to determine the GPFE of $L1_2$ Fe_3Ga by successive shear of every $(1\,1\,1)$ plane over $\frac{1}{6}[\bar{1}\,\bar{1}\,2]$ twinning partial (the twinning Burgers vector $b = \frac{\sqrt{6}}{6}a$, where a is the lattice parameter of 3.66 Å shown in table 1). Figure 8(*a*) shows the perfect $L1_2$ lattice of Fe_3Ga, while figure 8(*b*) is the lattice with a three-layer pseudotwin after shearing $3b$ (shown

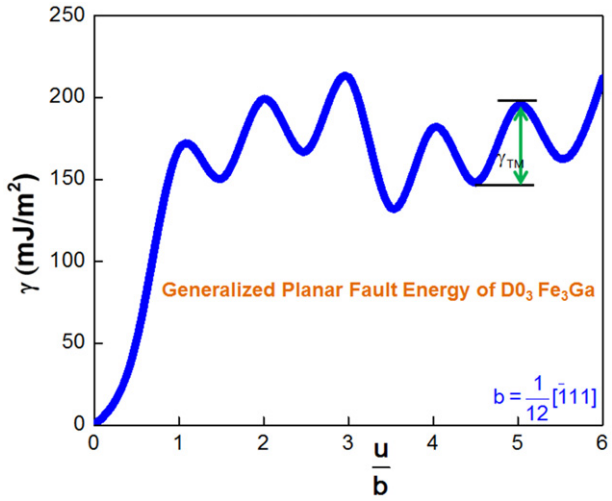

Figure 6. The GPFE curve in $(1\,\bar{1}\,2)$ plane with $\frac{1}{12}[\bar{1}\,1\,1]$ twinning dislocation of $D0_3$ Fe_3Ga. The twinning Burgers vector is $b = \frac{\sqrt{3}}{12}a_0$. The twin migration energy, γ_{TM}, shown with a green arrow indicates the difference between the stable and unstable stacking-fault energies.

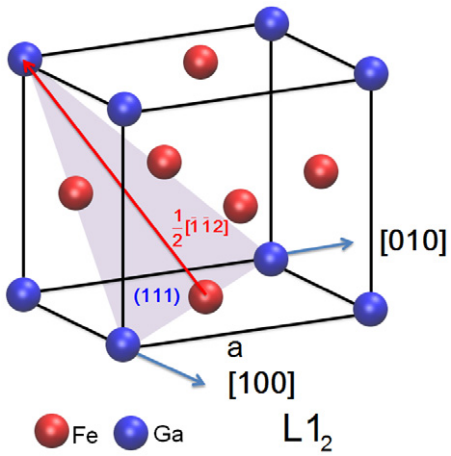

Figure 7. Pseudotwinning plane $(1\,1\,1)$ (shaded violet) and dislocation $[\bar{1}\,\bar{1}\,2]$ (red arrow) in $L1_2$ Fe_3Ga.

by a red arrow) in successive $(1\,1\,1)$ planes (twinning plane is marked with a brown dashed line). The atomic arrangement is viewed from the $[\bar{1}\,1\,0]$ direction. Similar to face-centered cubic (fcc) metals, the $L1_2$ is also a close-packed structure, and its atomic stacking sequence is ...ABCABCA... [42, 46–48]. We note that the twinning mechanism is different between fcc metals and $L1_2$ structures. It is well known that after the three-layer twin is formed, the atomic stacking sequence of ...ABCABCA... in a perfect fcc metal becomes the sequence of ...ABCACBA.... The second letter 'A' in the sequence is assumed as the twin plane, and the $(1\,1\,1)$ planes above it are displaced by shearing with $\frac{1}{6}[\bar{1}\,\bar{1}\,2]$ [19]. However, in a perfect

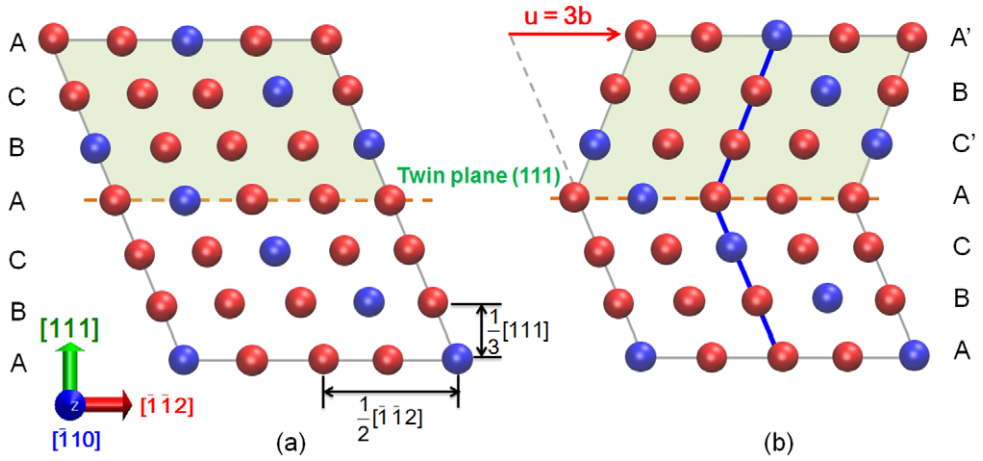

Figure 8. Pseudotwinning in (1 1 1) plane with partial dislocation $\frac{1}{6}[\bar{1}\,\bar{1}\,2]$ (twinning Burgers vector $b = 1.49$ Å) of $L1_2$ Fe_3Ga. (*a*) The perfect $L1_2$ lattice viewed from the $[\bar{1}\,1\,0]$ direction. Twining plane (1 1 1) is marked with a brown dashed line. (*b*) The lattice with a three-layer twin after shearing $3b$ along $\frac{1}{6}[\bar{1}\,\bar{1}\,2]$ shown with a red arrow. The stacking sequence of ... ABCABCA ... in a perfect $L1_2$ structure becomes the sequence of ... ABCAC′BA′ ... in a pseudotwin structure.

$L1_2$ structure the (1 1 1) planes above the twin plane have the transition B → C′ and A → A′. Here A′ and C′ represent the planes with the same lattice sites as planes A and C, but the lattice sites have different species of atoms. Thus, the stacking sequence of ... ABCABCA ... in a perfect $L1_2$ structure becomes the sequence of ... ABCAC′BA′ ... in a pseudotwin structure.

Figure 9 shows a unit cell of pseudotwin structure with 32 atoms transformed from the original $L1_2$ structure. The unit cell of the pseudotwin structure contains eight fcc subcells (one of them is shown in shaded violet and the left figure is the enlarged version), and these fcc subcells are different to the original $L1_2$ fcc unit cell shown in figure 7. We note that in the original $L1_2$ unit cell, the Ga atoms are located at corners and Fe atoms are at the face centers; while in the fcc subcell shown in figure 9, both the Ga and Fe atoms are located at specific corners and face centers keeping the atomic ratio 1 : 3.

We calculated the GPFE curve by shear of consecutive (1 1 1) layers by displacement, u, normalized by the twinning Burgers vector b along the $[1\,1\,\bar{2}]$ direction. The calculated energy landscape for a three-layer twin formation in $L1_2$ Fe_3Ga is shown in figure 10. We note that unlike the case of $D0_3$ Fe_3Ga, $u/b = 0.5$ is the unstable stacking-fault energy (maximum energy barrier of 512 mJ m^{-2}) for emitting the first twinning partial, and $u/b = 1$ corresponds to the intrinsic stacking-fault energy (metastable state). The calculated twin nucleation and migration energies are 644 mJ m^{-2} (at $u/b = 1.5$) and 340 mJ m^{-2}, respectively, which are much higher than the case of $D0_3$ Fe_3Ga. This indicates that pseudotwinning nucleation in $L1_2$ is more difficult and much higher stress is required to overcome these high energy barriers. However, we should note that if the applied stress is large enough (or if a high local stress concentration exists) to overcome these barriers, the pseudotwin in $L1_2$ can also be activated.

3. Twin nucleation model based on P–N formulation

It is now well known that a twin nucleus in metals and alloys is initiated by pre-existing dislocations, where multi-layered stacking fault structures are formed [49–51]. Experimental

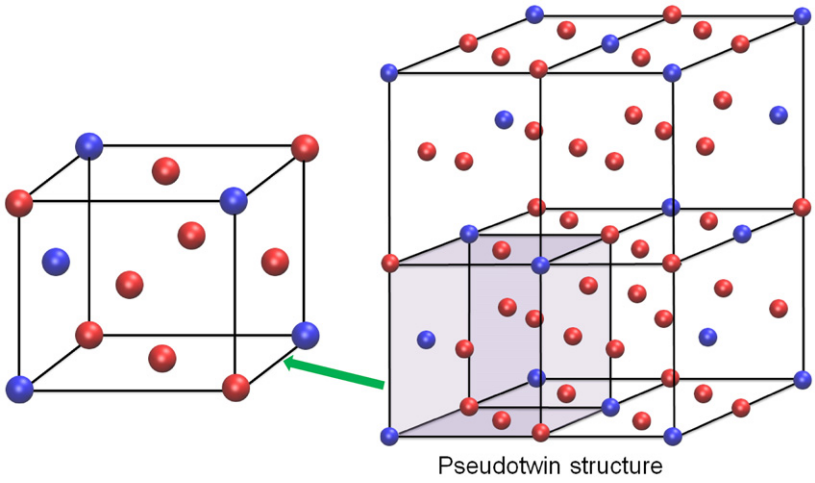

Figure 9. The unit cell of pseudotwin structure of $L1_2$. Upon pseudotwinning, the $L1_2$ lattice transforms to a pseudotwin structure with 32 atoms in one primitive unit cell. The unit cell of the pseudotwin structure contains eight fcc subcells (one of them is shown in violet and the left figure is the enlarged version), and these fcc subcells are different from the original $L1_2$ fcc unit cell shown in figure 7.

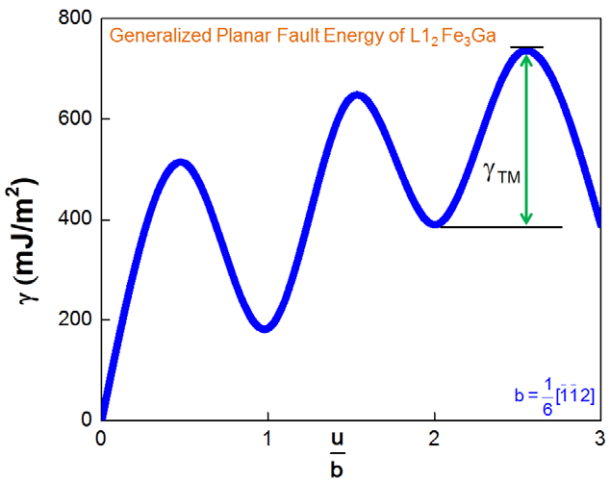

Figure 10. The GPFE curve in (1 1 1) plane with twinning dislocation $\frac{1}{6}[1\,1\,\bar{2}]$ of $L1_2$ Fe_3Ga. The shear displacement, u, is normalized by the twinning Burgers vector $b = \frac{1}{6}[\bar{1}\,\bar{1}\,2]$. The twin migration energy barrier, γ_{TM}, is 340 mJ m^{-2}.

evidence shows that the morphology of a twinning dislocation array near the twin tip is thin and semi-lenticularly shaped [51–54]. Figure 11 shows a schematic of the twin morphology [22]. Once the first twinning partial (leading twinning dislocation) has nucleated, subsequent partials readily form on successive twin planes [51, 55]. Thus, the critical step of twin nucleation is the activation of the first twinning partial dislocation in the twin plane involving an intrinsic stacking fault [50, 51, 54, 55]. This can occur in a region of high stress concentration such as inclusions, grain boundaries and notches [50]. In figure 11, h is the twin thickness and

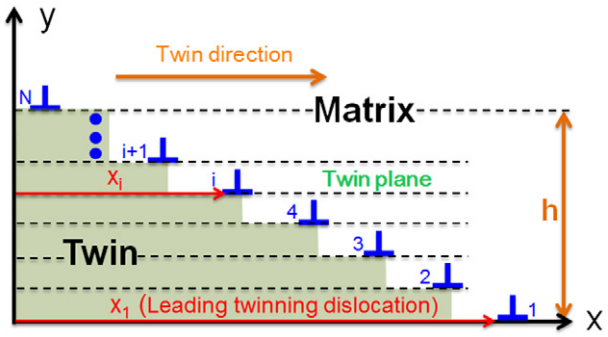

Figure 11. Schematic of a semi-lenticular twin morphology. h is the twin thickness and N is the number of twin layers. x_i is the position of ith twinning partial dislocation.

N is the number of twin layers, and x_i is the ith twinning partial's position. The minimum applied shear stress τ forming a twin is called critical twin nucleation stress, τ_{crit}. We seek for minimization of the total energy involved in the twin nucleus as described below.

Following the classical energetic approach for twin nucleus [50, 56, 57], the total energy associated with the twin nucleation shown in figure 11 can be expressed as

$$E_{\text{total}} = E_{\text{int}} + E_{\text{GPFE}} + E_{\text{line}} - W, \tag{1}$$

where E_{int} is the twin dislocation's interaction energy, E_{GPFE} is the twin boundary energy (GPFE), E_{line} is the twin dislocation's line energy and W is the applied work. These energy terms can be described as follows [22].

(1) Twinning dislocation's interaction energy, E_{int}

The interaction energy considering the dislocation's pile-up is given by [58, 59]

$$E_{\text{Inter}} = \frac{\mu b^2}{4\pi(1-\nu)}\left(1-\nu\cos^2\theta\right)\sum_{\substack{i=1\\ i>j=1}}^{N-1}\ln\frac{L}{x_i - x_j}. \tag{2}$$

(2) Twin boundary energy (GPFE), E_{GPFE}

Considering the interaction of multiple twinning partials, the disregistry function $f_{(x)}$ [22, 60, 61] can be described in the following expression:

$$f(x) = \frac{b}{2} + \frac{b}{N\pi}\left[\tan^{-1}\left(\frac{x-x_1}{\zeta}\right) + \tan^{-1}\left(\frac{x-x_2}{\zeta}\right) + \cdots + \tan^{-1}\left(\frac{x-x_N}{\zeta}\right)\right]. \tag{3}$$

In the GPFE curve, the energy required to create an intrinsic stacking fault can be expressed as

$$\gamma_{\text{SF}}\left(f(x)\right) = \gamma_{\text{isf}} + \left(\frac{\gamma_{\text{us}} - \gamma_{\text{isf}}}{2}\right)\left\{1 - \cos\left[2\pi\frac{f(x)}{b}\right]\right\} \quad \text{for } 0 \leqslant f(x) \leqslant b. \tag{4}$$

The energy required to nucleate a twin can be expressed as

$$\gamma_{\text{twin}}\left(f(x)\right) = \left(\frac{2\gamma_{\text{tsf}} + \gamma_{\text{isf}}}{2}\right) + \frac{1}{2}\left[\gamma_{\text{ut}} - \left(\frac{2\gamma_{\text{tsf}} + \gamma_{\text{isf}}}{2}\right)\right]\left\{1 - \cos\left[2\pi\frac{f(x)}{b}\right]\right\} \tag{5}$$

for $b < f(x) \leqslant Nb$.

Thus, the twin boundary energy E_{GPFE} based on P–N formulation [26, 60, 62] can be expressed as

$$E_{\mathrm{GPFE}} = \sum_{m=-\infty}^{+\infty} \gamma\left[f(mb)\right]b = \sum_{m=-\infty}^{+\infty} \gamma_{\mathrm{SF}}\left[f(mb)\right]b + (N-1)\sum_{m=-\infty}^{+\infty} \gamma_{\mathrm{twin}}\left[f(mb)\right]b. \tag{6}$$

(3) Dislocation line energy, E_{line}

$$E_{\mathrm{line}} = N\left[\frac{\mu b^2}{4\left(1-\nu\right)}\left(1-\nu\cos^2\theta\right)\right] = \frac{N\mu b^2}{4\left(1-\nu\right)}\left(1-\nu\cos^2\theta\right). \tag{7}$$

As we will see in the total energy expression, the dislocation line energy, E_{line}, does not depend on the spacing x_i, so it will not contribute to the critical twin nucleation stress [56, 57].

(4) Applied work, W

The applied work in the twin plane along the direction of the Burgers vector b is given as follows [63]:

$$W = \sum_{i=1}^{N} \tau b x_i. \tag{8}$$

When all the terms in the total energy expression are determined, the total energy for the twin nucleation can be expressed as follows:

$$\begin{aligned} E_{\mathrm{total}} &= E_{\mathrm{int}} + E_{\mathrm{GPFE}} + E_{\mathrm{line}} - W = \frac{\mu b^2}{4\pi\left(1-\nu\right)}\left(1-\nu\cos^2\theta\right)\sum_{\substack{i=1\\ i>j=1}}^{N-1} \ln\frac{L}{x_i - x_j} \\ &+ \sum_{m=-\infty}^{+\infty} \gamma_{\mathrm{SF}}\left[f(mb)\right]b + (N-1)\sum_{m=-\infty}^{+\infty} \gamma_{\mathrm{twin}}\left[f(mb)\right]b + \frac{N\mu b^2}{2\left(1-\nu\right)}\left(1-\nu\cos^2\theta\right) \\ &- \sum_{i=1}^{N} \tau b x_i. \end{aligned} \tag{9}$$

For a constant value of N in specific twin systems, the total energy is a function of x_i. To determine the critical twin nucleation stress, τ_{crit}, we minimized the total energy of the three-layer nucleus, E_{total}, with respect to x_i as follows:

$$\frac{\partial E_{\mathrm{total}}}{\partial x_i} = 0 \tag{10}$$

$$\begin{aligned} \frac{\partial E_{\mathrm{total}}}{\partial x_i} &= \frac{\mu b^2}{4\pi\left(1-\nu\right)}\left(1-\nu\cos^2\theta\right)\sum_{\substack{j=1\\ i\neq j}}^{N} \frac{1}{x_i - x_j} \\ &+ \frac{b}{N}\left\{\gamma_{\mathrm{us}} - \gamma_{\mathrm{isf}} + (N-1)\left[\gamma_{\mathrm{ut}} - \left(\frac{2\gamma_{\mathrm{tsf}} + \gamma_{\mathrm{isf}}}{2}\right)\right]\right\} \\ &\times \sum_{m=-\infty}^{m=\infty}\left[\frac{\zeta}{\zeta^2 + (mb - x_i)^2}\right] \times \sin\left\{\frac{2}{N}\left[\tan^{-1}\left(\frac{mb - x_1}{\zeta}\right)\right.\right. \\ &\left.\left. + \cdots + \tan^{-1}\left(\frac{mb - x_N}{\zeta}\right)\right]\right\} - \tau b = 0, \qquad (i = 1, 2, \ldots, N). \end{aligned} \tag{11}$$

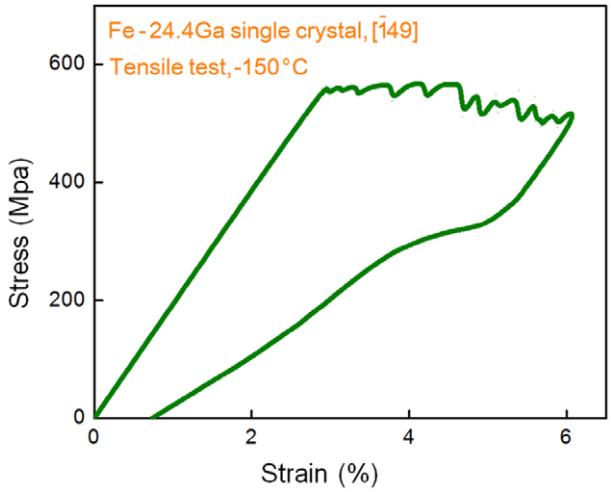

Figure 12. Stress–strain curve of Fe-24.4Ga single-crystal tensile tests at −150 °C [17]. The recoverability is attributed to the formation of pseudotwins and return to the original crystal structure upon unloading.

Then the explicit expression for the twinning stress is given by

$$\tau = \frac{\mu b}{4\pi(1-\nu)}\left(1-\nu\cos^2\theta\right)\sum_{\substack{j=1\\ i\neq j}}^{N}\frac{1}{x_i-x_j} + \frac{1}{N}\left\{\gamma_{\mathrm{us}}-\gamma_{\mathrm{isf}}+(N-1)\left[\gamma_{\mathrm{ut}}-\left(\frac{2\gamma_{\mathrm{tsf}}+\gamma_{\mathrm{isf}}}{2}\right)\right]\right\} \times \sum_{m=-\infty}^{m=\infty}\left[\frac{\zeta}{\zeta^2+(mb-x_i)^2}\right]\times\sin\left\{\frac{2}{N}\left[\tan^{-1}\left(\frac{mb-x_1}{\zeta}\right)+\cdots+\tan^{-1}\left(\frac{mb-x_N}{\zeta}\right)\right]\right\}, \qquad (i=1,2,\ldots,N). \tag{12}$$

4. Discussion

By numerically solving equation (12) for $N = 3$, we calculated the critical twin nucleation stress, $\tau_{\mathrm{crit}} = 235$ MPa, for a pseudotwin of $D0_3$ Fe_3Ga. The corresponding equilibrium spacing between two adjacent partials are $d_1 = 35$ Å and $d_2 = 55$ Å with $d_1 = x_1 - x_2$ and $d_2 = x_2 - x_3$ ($x_1 = 560$ Å, $x_2 = 525$ Å, $x_3 = 470$ Å). Figure 12 shows a stress–strain curve of Fe-24.4 Ga single-crystal tensile tests at −150 °C [17]. The loading axis of the specimens was at $[\bar{1}\,4\,9]$ orientation with a Schmid factor of 0.438 for the twinning system $(1\,\bar{1}\,2)[\bar{1}\,1\,1]$. We note that the predicted critical twin nucleation stress of 235 MPa in $D0_3$ Fe_3Ga is in good agreement with available experimental measurements of 225–249 MPa [17, 64].

We also calculated the critical twin nucleation stress in $L1_2$ Fe_3Ga as 492 MPa based on the proposed model, which is much higher than the $D0_3$ case and is unlikely to be observed experimentally. The 'ideal twin stress' can be calculated by the maximum slope of the GPFE curve with respect to the shear displacement and in the form of $\tau_{\mathrm{ideal}} = \pi\{\gamma_{\mathrm{TM}}/b\}$ [41]. We compared the critical twin nucleation stress, τ_{crit}, for $D0_3$ and $L1_2$ Fe_3Ga predicted from our P–N formulation based twin nucleation model with the 'ideal twin stress', τ_{ideal}, and

Table 2. The predicted critical twin nucleation stress, τ_{crit}, is compared to the ideal twin stress, $\tau_{TM\ ideal}$, and available experimental data in Fe_3Ga. The pseudotwinning system and Burgers vector are also given.

			Twinning stress (MPa)		
Structure of Fe_3Ga	Pseudotwinning system	Burgers vector b (Å)	Ideal twin stress, τ_{ideal}	Critical twin stress τ_{crit} (equation (12))	Experiments
$D0_3$	$\frac{1}{12}[\bar{1}\,1\,1](1\,\bar{1}\,2)$	0.84	1860	235	225–249 [17, 64]
$L1_2$	$\frac{1}{6}[1\,1\,\bar{2}](1\,1\,1)$	1.49	7160	492	—

Note:—indicates the experimental data is not available.

available experimental twinning stress data in table 2. We note that the ideal twin stress of 1860 MPa for $D0_3$ is nearly an order of magnitude larger than the twin nucleation stress observed experimentally. In contrast, our predicted critical twin stress of 235 MPa shows favorable agreement between experiment and the present theory. Similarly for the $L1_2$ case, the ideal twin stress of 7160 MPa is much larger than the predicted critical twin stress of 492 MPa. This observation demonstrates that the P–N formulation based twin nucleation model provides an accurate prediction of the twin nucleation stress.

Similar to the γ'Ni-based superalloys in $L1_2$ structure [42, 65–67], the true twin in $L1_2$ Fe_3Ga can be formed through the pseudotwin structure via atomic shuffling at high temperatures. This indicates that the shuffling, as a thermally activated reordering process, can reduce the formation energy of twins in $L1_2$ Fe_3Ga. The formation of a true twin in $L1_2$ Fe_3Ga includes two steps: (1) the formation of a pseudotwin; (2) the atomic shuffling on every two neighboring (1 1 1) planes of the pseudotwin. Our DFT simulations show that the structural energies are −7.087 eV/atom and −7.099 eV/atom for $L1_2$ pseudotwin structure and true-twin structure, respectively. This result indicates that atomic shuffling can make the true-twin structure more energetically stable than pseudotwin structure. However, the atomic shuffling required to maintain mirror symmetry hardly occurs at low temperatures and formation of pseudotwin is favored instead [17]. Furthermore, we note that a different deformation mechanism to form the true twin in $L1_2$ Fe_3Ga has been proposed [45]. This so-called anti-twinning mode occurs by the movement of $\frac{1}{3}[1\,1\,\bar{2}]$ partials on successive (1 1 1) planes. Our DFT simulations show that the unstable stacking-fault energy for emitting the first anti-twinning partial is 2588 mJ m^{-2}, which is significantly higher than the energy for pseudotwin of 512 mJ m^{-2} shown in figure 10, ruling out this anti-twinning deformation mode.

We note that the pseudotwin in $D0_3$ and $L1_2$ structures is formed without atomic shuffling [42, 45, 64, 65]. However, the full internal atomic relaxation associated with twinning shear takes place during twin formation. The DFT simulations in the paper, involving displacements in the parallel and normal directions to the twin plane, provided more accurate energy barriers (GPFE). The additional atomic displacement due to full relaxation is very small and its magnitude is calculated within 1% of the twinning Burgers vector. Compared to the energy barrier for relaxation perpendicular to the twin plane, the energy barriers after full relaxation can be nearly 10% smaller [22]. We should note that this relaxation is different to atomic shuffling. Atomic shuffling involves interchanges between atoms to restore the original crystal structure during twin formation (for example, atomic shuffling in $L1_2$ Fe_3Ga transforms the pseudotwin to the true twin). However, atomic relaxation maintains the pseudotwin structure while reducing the energy barrier in twin formation.

5. Summary

In the present work, we calculated the pseudotwin energy landscape and twinning stress in $D0_3$ and $L1_2$ Fe_3Ga, and discussed why pseudotwinning is more favored in $D0_3$ than $L1_2$. In this paper, we showed very favorable predictions of experimental twinning stress with the proposed theory. Therefore, the modeling represents a significant advancement to understanding of pseudotwinning in Fe_3Ga. Pseudotwinning results in a new phase formed where the crystal structure of the ordered lattice is not retained in the twinned lattice. Thus, pseudotwinning is like a martensitic transformation, where the ordered lattice transforms to the pseudotwin phase. The pseudotwin in cubic $D0_3$ results in an orthorhombic structure; while in cubic $L1_2$ it results in a new superlattice containing eight fcc subcells. We precisely established the twinning energy pathway of $D0_3$ and $L1_2$ Fe_3Ga, utilizing first-principles calculations. Energy barriers for pseudotwin formation are quantified with the GPFE curves for different twinning systems in $D0_3$ and $L1_2$ Fe_3Ga. The GPFE in $D0_3$ is similar to the pattern of bcc metals, while the GPFE in $L1_2$ is similar to the pattern of fcc metals. We illustrated that energy barriers of pseudotwin nucleation and migration in $L1_2$ are significantly higher than the barriers in $D0_3$, which would require very high applied stress to overcome. To determine twin nucleation stresses of pseudotwin formation in Fe_3Ga, we present a pseudotwin nucleation model based on the Peierls–Nabarro formulation incorporating atomistic simulations and groups of dislocation bounding the twin nucleus. This model links the mesoscale twinning partial dislocation interactions using dislocation mechanics and lattice shears at atomistic scale. We minimize the total energy associated to pseudotwin nucleation and calculate the critical twin nucleation stress of $D0_3$ and $L1_2$ Fe_3Ga. Through the calculation results, we found that the twin nucleation stress in $D0_3$ of 235 MPa is one-half of the stress in $L1_2$ of 495 MPa. The very high twin nucleation stress makes pseudotwinning in $L1_2$ less favored. We verified the predictions with available experiments measuring the twinning stress in $D0_3$ Fe_3Ga with excellent agreement.

In summary, the present work is geared towards the quantification of pseudotwin energy barriers and the prediction of twinning stresses in $D0_3$ and $L1_2$ Fe_3Ga. The results explain why pseudotwinning in $D0_3$ Fe_3Ga has been observed experimentally. We suggest that the results can serve as the foundation to develop a methodology to understanding and determining pseudotwinning in ordered lattice.

Acknowledgment

The support of National Science Foundation grant CMMI-1300284 is gratefully acknowledged.

References

[1] Christian J W and Mahajan S 1995 Deformation twinning *Prog. Mater. Sci.* **39** 1
[2] Singh J B, Sundararaman M and Krishnan M 2011 The nature of pseudo-twinning modes on the basis of a twin classification scheme *Scr. Mater.* **64** 371–3
[3] Chumlyakov Y *et al* 2008 High-temperature superelasticity in CoNiGa, CoNiAl, NiFeGa, and TiNi monocrystals *Russ. Phys. J.* **51** 1016–36
[4] Goo E, Duerig T, Melton K and Sinclair R 1985 Mechanical twinning in $Ti_{50}Ni_{47}Fe_3$ and $Ti_{49}Ni_{51}$ alloys *Acta Metall.* **33** 1725
[5] Moberly W J, Proft J L, Duerig T W, Pelton A R and Sinclair R 1991 *Thermomechanical Strengthening of B2 Intermetallics* (New Orleans, LA: Minerals, Metals & Materials Society (TMS)) pp 387

[6] Moberly W J, Proft J L, Duerig T W and Sinclair R 1990 Deformation, twinning and thermo-mechanical strengthening of $Ti_{50}Ni_{47}Fe_3$ *Acta Metall. Mater.* **38** 2601
[7] Nishida M, Matsuda M, Fujimoto T, Tanka K, Kakisaka A and Nakashima H 2006 Crystallography of deformation twin boundaries in a B2 type Ti–Ni alloy *Mater. Sci. Eng.* A **438–440** 495
[8] Laves F 1952 Mechanische Zwillingsbildung in Feldspäten in Abhängigkeit von Ordnung-Unordnung der Si/Al-Verteilung innerhald des (Si, Al) 4 O 8-Gerüstes *Naturwissenschaften* **39** 546–7
[9] Cahn R 1954 Twinned crystals *Adv. Phys.* **3** 363–445
[10] Chou T-W 1975 Elastic interactions between disclination loops and dislocations *J. Appl. Phys.* **46** 523–7
[11] Laves F 1966 What is a twin and what is a 'twin'? *Acta Metall.* **14** 58
[12] Green M L and Cohen M 1979 Pseudotwinning and pseudoelasticity in β Fe–Be alloys *Acta Metall.* **27** 1523–38
[13] Yang S, Hou D, Shyue J, Wheeler R and Fraser H 1995 Pseudo-twinning in a deformed Nb–15Al–25Ti B2 alloy *Mater. Res. Soc. Symp. Proc.* **364** 1359–64
[14] Ezaz T and Sehitoglu H 2011 Coupled shear and shuffle modes during twin growth in B2-NiTi *Appl. Phys. Lett.* **98** 241906
[15] Paxton A T 1995 Impossibility of pseudotwinning in B2 alloys *Acta Metall. Mater.* **43** 2133–6
[16] Yasuda H Y, Oda Y, Kishimoto T and Maruyama T 2012 Effect of Ga concentration on twinning pseudoelasticity in Fe–Ga single crystals *J. Alloys Compounds* **577** 5563–7
[17] Yasuda H Y, Kishimoto T and Umakoshi Y 2010 Temperature dependence of twinning pseudoelasticity in Fe_3Ga single crystals *Mater. Trans.* **51** 2196
[18] Yasuda H Y, Oda Y, Aoki M, Fukushima K and Umakoshi Y 2008 Multimode pseudoelasticity in Fe–23.8 at% Ga single crystals with $D0_3$ structure *Intermetallics* **16** 1298–304
[19] Kibey S, Liu J B, Johnson D D and Sehitoglu H 2007 Predicting twinning stress in fcc metals: linking twin-energy pathways to twin nucleation *Acta Mater.* **55** 6843
[20] Ezaz T, Sehitoglu H and Maier H J 2012 Energetics of (1 1 4) twinning in B2 NiTi under coupled shear and shuffle *Acta Mater.* **60** 339–48
[21] Vitek V 1968 Intrinsic stacking faults in body-centred cubic crystals *Phil. Mag.* **18** 773
[22] Wang J and Sehitoglu H 2013 Twinning stress in shape memory alloys: theory and experiments *Acta Mater.* **61** 6790–801
[23] Nabarro F R N 1952 Mathematical theory of stationary dislocations *Adv. Phys.* **1** 269–394
[24] Nabarro F R N 1947 Dislocation in a simple cubic lattice *Proc. Phys. Soc.* **59** 256–72
[25] Nabarro F R N and Duesbery M S 2002 *Dislocations in Solids* (Amsterdam: Elsevier)
[26] Joós B and Duesbery M S 1997 The Peierls stress of dislocations: an analytic formula *Phys. Rev. Lett.* **78** 266–9
[27] Yasuda H Y, Aoki M and Umakoshi Y 2007 Effect of the ordering process on pseudoelasticity in Fe_3Ga single crystals *Acta Mater.* **55** 2407–15
[28] Müllner P and Pirouz P 1997 A disclination model for the twin–twin intersection and the formation of diamond-hexagonal silicon and germanium *Mater. Sci. Eng.* A **233** 139–44
[29] Kang K, Bulatov V V and Cai W 2012 Singular orientations and faceted motion of dislocations in body-centered cubic crystals *Proc. Natl Acad. Sci. USA* **109** 15174–8
[30] Schoeck G 2011 The Peierls stress in a simple cubic lattice *Phys. Status Solidi* b **248** 2284–9
[31] Kresse G and Furthmuller J 1996 Efficient iterative schemes for *ab initio* total-energy calculations using a plane-wave basis set *Phys. Rev.* B **54** 11169
[32] Kresse G and Hafner J 1993 *Ab initio* Hellmann–Feynman molecular dynamics for liquid metals *J. Non-Cryst. Solids* **156** 956–60
[33] Fu C L and Yoo M H 1992 Deformation behavior of B2 type aluminides: FeAl and NiAl *Acta Metall. Mater.* **40** 703–11
[34] Paidar V 1976 Generalized stacking faults in model lattice of ordered Fe–Si alloys *Czech. J. Phys.* **26** 865–74
[35] Juan Y-M and Kaxiras E 1996 Generalized stacking fault energy surfaces and dislocation properties of silicon: a first-principles theoretical study *Phil. Mag.* A **74** 1367–84

[36] Cohen J and Weertman J 1963 A dislocation model for twinning in fcc metals *Acta Metall.* **11** 996–8
[37] Srisukhumbowornchai N and Guruswamy S 2002 Influence of ordering on the magnetostriction of Fe–27.5 at% Ga alloys *J. Appl. Phys.* **92** 5371–9
[38] Srisukhumbowornchai N and Guruswamy S 2001 Large magnetostriction in directionally solidified FeGa and FeGaAl alloys *J. Appl. Phys.* **90** 5680–8
[39] Suzuki T, Oya Y and Ochiai S 1984 The mechanical behavior of nonstoichiometric compounds Ni_3Si, Ni_3Ge, and Fe_3Ga *Metall. Trans.* A **15** 173–81
[40] Li S *et al* 2010 Superelasticity in bcc nanowires by a reversible twinning mechanism *Phys. Rev.* B **82** 205435
[41] Ogata S, Ju L and Yip S 2005 Energy landscape of deformation twinning in bcc and fcc metals *Phys. Rev.* B **71** 224102
[42] Xie H-X, Bo L and Yu T 2012 Atomistic simulation of microtwinning at the crack tip in $L_{12}Ni_3Al$ *Phil. Mag.* **92** 1542–53
[43] Xie H-X, Wang C-Y, Yu T and Du J-P 2009 Condensed matter: structure, thermal and mechanical properties: dislocation formation and twinning from the crack tip in Ni_3Al: molecular dynamics simulations *Chin. Phys.* B **18** 251–8
[44] Yoo M 1989 Deformation twinning in superlattice structures *J. Mater. Res.* **4** 50–4
[45] Chu F and Pope D P 1993 Deformation twinning in intermetallic compounds—the dilemma of shears versus shuffles *Mater. Sci. Eng.* A **170** 39–47
[46] Mahajan S and Chin G Y 1973 *Formation of Deformation Twins in FCC Crystals* (New York: Metallurgical Society AIME) pp 47
[47] Yamaguchi M, Vitek V and Pope D 1981 Planar faults in the L12, lattice stability and structure *Phil. Mag.* A **43** 1027–44
[48] Chandran M and Sondhi S 2011 First-principle calculation of APB energy in Ni-based binary and ternary alloys *Modelling Simul. Mater. Sci. Eng.* **19** 025008
[49] Liu Y and Yang H 1999 The concern of elasticity in stress-induced martensitic transformation in NiTi *Mater. Sci. Eng.* A **260** 240–5
[50] Marcinkowski M and Sree Harsha K 1968 Numerical analysis of deformation twin behavior. Small static twin lamellas *J. Appl. Phys.* **39** 6063–70
[51] Jin Z and Bieler T R 1995 An *in-situ* observation of mechanical twin nucleation and propagation in TiAl *Phil. Mag.* A **71** 925–47
[52] Zhang L 1999 Twin-intersection-related nanotwinning in a heavily deformed gamma-TiAl-based alloy *Phil. Mag. Lett.* **79** 49–54
[53] Müllner P and Romanov A 2000 Internal twinning in deformation twinning *Acta Mater.* **48** 2323–37
[54] Gutkin M Y, Ovid'ko I and Skiba N 2007 Mechanism of deformation-twin formation in nanocrystalline metals *Phys. Solid State* **49** 874–82
[55] Appel F, Paul J D H and Oehring M 2011 *Gamma Titanium Aluminide Alloys: Science and Technology* (New York: Wiley)
[56] Cooper R 1965 The equilibrium shape of deformation twins *Acta Metall.* **13** 46–8
[57] Cooper R 1966 The equilibrium shape of deformation twins: II *Acta Metall.* **14** 78–80
[58] Lazar P and Naturarum D R 2006 *Ab Initio Modelling of Mechanical and Elastic Properties of Solids* (Vienna: University of Vienna)
[59] Dundurs J 1969 *Mathematical Theory of Dislocations* (New York: American Society of Mechanical Engineers) pp 70–115
[60] Joós B, Ren Q and Duesbery M S 1994 Peierls–Nabarro model of dislocations in silicon with generalized stacking-fault restoring forces *Phys. Rev.* B **50** 5890–8
[61] Carrez P, Ferré D and Cordier P 2009 Peierls–Nabarro modelling of dislocations in MgO from ambient pressure to 100 GPa *Modelling Simul. Mater. Sci. Eng.* **17** 035010
[62] Nabarro F R N 1997 Theoretical and experimental estimates of the Peierls stress *Phil. Mag.* A **75** 703–11
[63] Cherkaoui M and Capolungo L 2009 Atomistic and Continuum Modeling of Nanocrystalline Materials: Deformation Mechanisms and Scale Transition (Berlin: Springer)

[64] Yasuda H Y, Aoki M, Oda Y, Fukushima K and Umakoshi Y 2009 Unusual pseudoelastic behaviour of Fe_3Ga shape memory alloys *Int. Conf. on Advanced Structural and Functional Materials Design (Osaka, 10–12 November 2008)* (Bristol: IOP Publishing) pp 012053 (6pp)

[65] Kolbe M 2001 The high temperature decrease of the critical resolved shear stress in nickel-base superalloys *Mater. Sci. Eng.* A **319** 383–7

[66] Viswanathan G, Karthikeyan S, Sarosi P, Unocic R and Mills M 2006 Microtwinning during intermediate temperature creep of polycrystalline Ni-based superalloys: mechanisms and modelling *Phil. Mag.* **86** 4823–40

[67] Kovarik L *et al* 2009 Microtwinning and other shearing mechanisms at intermediate temperatures in Ni-based superalloys *Prog. Mater. Sci.* **54** 839–73